IEEE Access
Multidisciplinary | Rapid Review | Open Access Journal

Received January 30, 2020, accepted February 15, 2020, date of publication February 27, 2020, date of current version March 10, 2020.

Digital Object Identifier 10.1109/ACCESS.2020.2976780

Single-Fed Circularly Polarized Dielectric Resonator Antenna With an Enhanced Axial Ratio Bandwidth and Enhanced Gain

SON TRINH-VAN, YOUNGOO YANG, (Member, IEEE), KANG-YOON LEE, AND KEUM CHEOL HWANG, (Senior Member, IEEE)

Department of Electrical and Computer Engineering, Sungkyunkwan University, Suwon 440-746, South Korea

Corresponding author: Keum Cheol Hwang (khwang@skku.edu)

This work was supported by the National Research Foundation of Korea (NRF) Grant funded by the Korean Government, Ministry of Science and ICT (MSIT) under Grant 2014R1A5A1011478.

ABSTRACT A compact single-fed circularly polarized dielectric resonator antenna (DRA) with an enhanced 3-dB axial ratio bandwidth (ARBW) and gain is proposed. The DRA is implemented by joining a smaller dielectric resonator (DR) to one side wall of a main rectangular DR and is excited by an offset vertical metallic strip. With this configuration, two sets of degenerate orthogonal modes, the TE_{111} mode and TE_{113} mode, are simultaneously excited to realize wideband circular polarization operation. Furthermore, by removing a small DR portion from the lower corner of the main DR, the boresight gains at higher frequencies are significantly enhanced. An antenna prototype is fabricated and measured to verify the performance of the proposed design. The experimental results illustrate that the proposed antenna achieves a measured 3-dB ARBW of approximately 44.73% (3.68–5.80 GHz) in conjunction with a broad −10 dB impedance bandwidth of 69.66% (2.9–6.0 GHz). The measured boresight gain is found to be 5.49±0.85 dBic within the passband with a maximum value of 6.34 dBic at 4.7 GHz. Moreover, reasonable agreement between the simulated and measured results is achieved.

INDEX TERMS Bandwidth enhancement, circular polarization, dielectric resonator antenna, higher order mode, wideband antenna.

I. INTRODUCTION

A dielectric resonator (DR) fabricated with a low-loss and high-permittivity material was implemented for the first time as an antenna by Long *et al.* [1] in 1983. Since then, dielectric resonator antennas (DRAs) have become very popular radiators for applications at microwave frequencies. With the absence of inherent conductor losses and surface waves, the DRA achieves higher radiation efficiency than a microstrip antenna. In addition, the DRA has other attractive features, such as a wide bandwidth, a simple mean of excitation, and versatility with regard to its shape and material. These attractive features make the DRA an excellent antenna candidate for modern wireless communication systems [2], [3]. Specifically, DRAs with circularly polarized (CP) radiation are preferred for such systems, as CP antennas, compared to linearly polarized (LP) antennas, are less affected by multipath interference and by misalignment between the transmitting and receiving antennas [4]. As a result, the design of the CP DRA has been subject of increased amounts of interest, as noted in several studies [4]–[19].

The generation of the orthogonal degenerate modes is typically required in the antenna structure to realize circular polarization. In CP DRAs, the required orthogonal degenerate modes can be generated either by single-point or multi-point feeding techniques [3]. A multi-point feed CP DRA can achieve a wider 3-dB axial ratio bandwidth (ARBW) but also requires an external feeding network, such as a power divider or hybrid coupler, resulting in an inevitable increase in the overall size, greater losses, and greater complexity of the

The associate editor coordinating the review of this manuscript and approving it for publication was Qingfeng Zhang.

antenna system as well [5], [6]. In contrast, single-point feed CP DRA has a simpler structure but usually gives a narrower 3-dB ARBW (typically 3-6%) [7]–[9]. Therefore, a variety of techniques have been reported to broaden the 3-dB ARBW of a single-feed CP DRA. For example, with two concentric open half-loops to excite a rectangular DR, a 3-dB ARBW of approximately 13% with a gain of 5 dBic was reported [10]. In other work [11], a 3-dB ARBW of 23.75% and a useful gain of 4.23 dBic were achieved by combining the CP bands of a Spidron fractal slot antenna and a grooved DR. In another study [12], a rectangular DR excited by a modified cross-slot leading to a wide 3-dB ARBW of 24.6% and a gain of more than 5 dBic was presented. Two vertical microstrip lines arranged in a perpendicular fashion were also implemented to excite a cylindrical DR [13], reportedly showing a 3-dB ARBW of 24.6% with an average gain of 5.5 dBic. Another approach is to fabricate DRs with special geometries. For example, a pixelated DR composed of 8 × 8 grid DR bars with different heights fed by a narrow rectangular slot was introduced, offering a 14.63% 3-dB ARBW with a peak gain of 6.13 dBi [14]. Pan et al. presented a trapezoidal DRA excited by an inclined slot to attain a 3-dB ARBW of 21.5% and a peak gain of 8.39 dBic [15]. Fakhte et al. used an inverted trapezoidal probe to excite a stair-shaped DRA, resulting in a wide 3-dB ARBW of 22% with a useful gain of 5.7 dBic [16]. Moreover, the aforementioned techniques can be combined to enhance the CP bandwidth of DRAs further. Several CP DRAs with a wide 3-dB ARBW of more than 40% have been reported. By using a stair-shaped coupling slot [17] and a vertical strip feedline [18] to excite multiple DR elements, wide 3-dB ARBWs of 41.01% and 44.2% were attained, respectively. However, in these designs, the use of a large slot on the ground plane [17] and/or partial ground plane [18] resulted in bidirectional radiation patterns. In a recent study [19], a single fed wideband CP DRA with a 3-dB ARBW of approximately 46.9% and a peak gain of 4.73 dBic realized by implementing four vertical metallic plates around a square DR was reported. This design, however, inevitably increases both the antenna footprint and the complexity.

In this article, a wideband single-fed CP DRA simply excited by an offset vertical metallic strip is proposed. By adding a smaller DR to the sidewall of the main rectangular DR, both the fundamental TE_{111} and the higher order TE_{113} modes are effectively excited and their CP modes are merged, resulting in an increase of approximately two times in the CP bandwidth as compared to that achieved solely with a rectangular DR. In addition, a small DR portion from the lower corner of the main rectangular DR is also removed to increase the radiation from the side walls [21], thus significantly enhancing the broadside gain at higher frequencies. As a result, a maximum enhancement of up to 3.0 dBic in the boresight gain is attained at 5.5 GHz. The performance of the proposed CP DRA is initially investigated and simulated in CST Microwave Studio using the finite-integration technique in the time-domain and is later experimentally validated through a fabricated prototype. Reasonable agreement is achieved between the simulated and measured results.

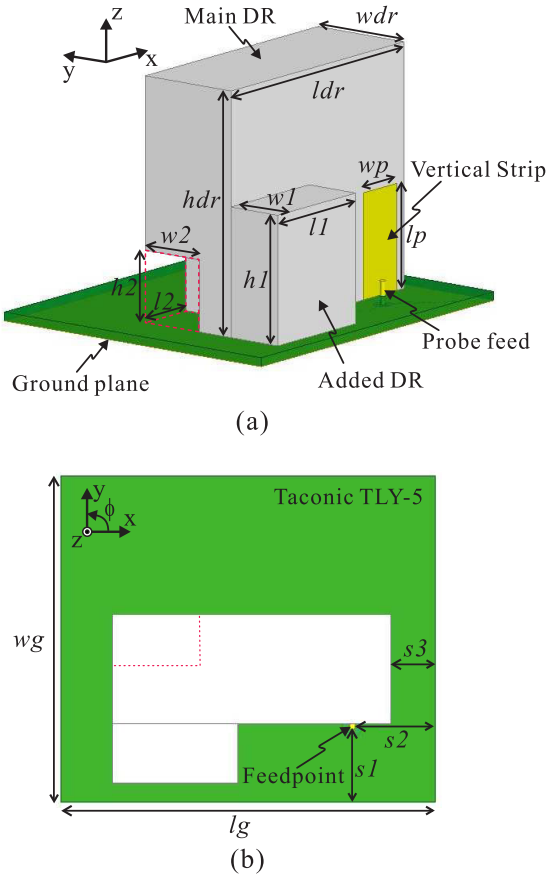

FIGURE 1. Configuration of the proposed CP DRA. (a) Perspective view. (b) Top view. ($wg = 27.5$, $lg = 31.5$, $wdr = 9.2$, $ldr = 23.41$, $hdr = 25.78$, $w1 = 5$, $l1 = 10.57$, $h1 = 11.25$, $w2 = 5.8$, $l2 = 5.5$, $h2 = 6.2$, $wp = 4.5$, $lp = 9.22$, $s1 = 6.4$, $s2 = 6.97$, $s3 = 3.75$. Units: mm).

Section II describes the antenna configuration. Section III presents the design procedure, operation mechanism, and bandwidth and gain enhancement techniques. The experimental results of the fabricated antenna are summarized and discussed in Section IV. Lastly, important conclusions are drawn in Section V.

II. ANTENNA CONFIGURATION

Figure 1 presents an illustration of the configuration of the proposed CP DRA. The proposed antenna structure includes a Taconic TLY-5 ($\epsilon_r = 2.2$, $\tan\delta = 0.0009$) dielectric substrate with dimensions $lg \times wg$ and a thickness of 0.76 mm. The ground plane is mounted on the bottom layer of the substrate. The main rectangular DR, which is made of a ceramic material with permittivity of 10, has dimensions of $ldr \times wdr \times hdr$ and is positioned on the top surface of the substrate at the position determined by the design parameters $s1$ and $s3$. A small DR dimensions of $l1 \times w1 \times h1$ is added to the sidewall of the main DR. A small DR portion $l2 \times w2 \times h2$ in size, indicated here the dashed red area, is removed from the left lower corner of the main DR. A metallic strip with

a width of wp and a length of lp is adhered vertically to the sidewall of the main DR to excite the proposed DRA. A probe feed is connected at the center of the vertical strip at the position determined by the design parameters $s1$ and $s2$. The design parameters of the proposed antenna are optimized to maximize the CP bandwidth, a determined by the criteria of $|S_{11}| \leq -10$ dB and AR ≤ 3 dB. The optimized geometrical parameters of the proposed antenna are shown in the caption of Figure 1.

III. ANTENNA OPTIMIZATION

Three different design configurations were considered during the design process, leading to the final design, as presented in Figure 2. Antenna I is a rectangular DRA excited by an offset vertical metallic strip to generate CP operation. Antenna II is implemented by adding a smaller DR to the sidewall of the main DR in Antenna I to broaden the 3-dB ARBW. Finally, the proposed antenna is realized by removing a small DR portion from a corner of the main DR in Antenna II to enhance the boresight gain.

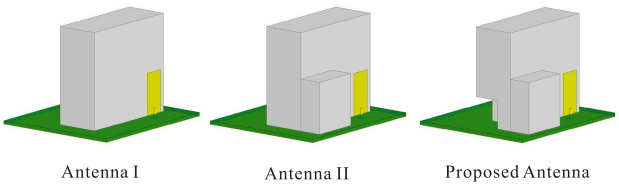

FIGURE 2. Methodology adopted to design the proposed CP DRA.

1) AXIAL RATIO BANDWIDTH ENHANCEMENT

This subsection presents the technique used to broaden the 3-dB ARBW. The design process starts with Antenna I. The dimensions of the main rectangular DR in Antenna I, $ldr \times wdr \times hdr$, are set to 23.41 mm × 9.2 mm × 25.78 mm such that the main rectangular DR operates with the fundamental TE_{111} and the higher order TE_{113} modes. The vertical metallic strip has a width of $wp = 4.5$ mm and a length of $lp = 9.22$ mm. The feed point location is defined as $s1 = 6.60$ mm and $s2 = 5.36$ mm. With this offset feeding configuration, the two orthogonal degenerate mode pairs of the TE_{111} (TE^x_{111} and TE^y_{111}) and TE_{113} (TE^x_{113} and TE^y_{113}), responsible for the generation of the CP wave, can be excited. As the dimensions of the main DR along the x-axis and y-axis differ, the resonant frequencies for a pair of similar modes will also differ. Using the dielectric waveguide model (DWM) [20], the resonant frequencies of the main rectangular DR are estimated to be 3.21 GHz (TE^y_{111}), 4.41 GHz (TE^y_{113}), 5.48 GHz (TE^x_{111}), and 6.08 GHz (TE^x_{113}). A full-wave simulation is conducted for Antenna I. Simulated results of the reflection coefficient and AR performance of Antenna I are shown in Figure 3. As observed, Antenna I achieves a wide −10 impedance bandwidth of 2.96–6.17 GHz with several dips found at 3.3 GHz, 4.4 GHz, 5.1 GHz, and 6.1 GHz. The simulated electric fields at these four frequencies are illustrated in Figure 4. The modes observed at 3.3 GHz and 5.1 GHz are identified

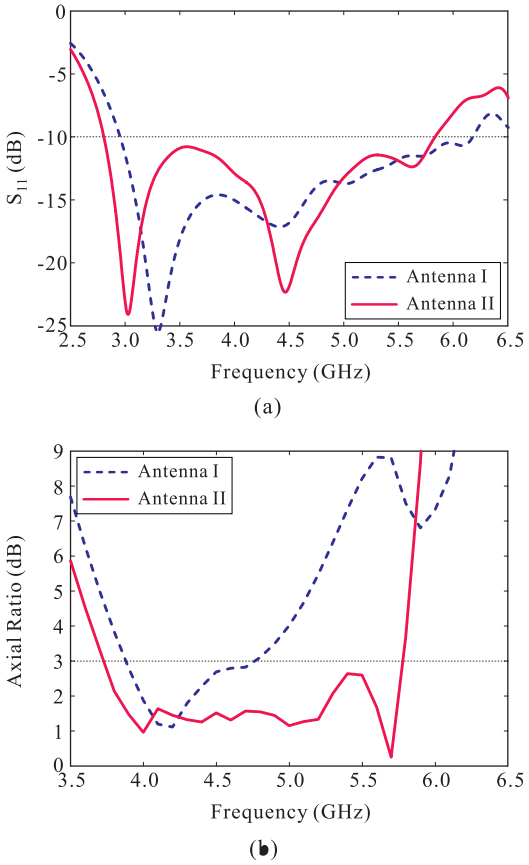

FIGURE 3. Simulated results of Antenna I and Antenna II. (a) Reflection coefficients and (b) axial ratios.

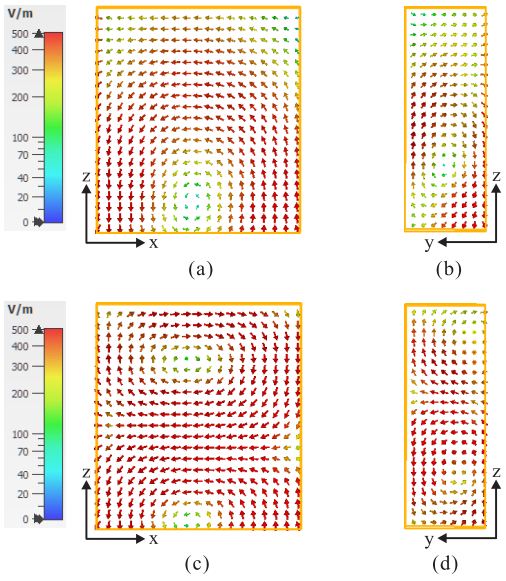

FIGURE 4. Simulated electric fields of Antenna I (a) TE^y_{111} at 3.3 GHz, (b) quasi-TE^x_{111} at 5.1 GHz, (c) TE^y_{113} at 4.4 GHz, and quasi-TE^x_{113} at 6.1 GHz.

as the TE^y_{111} and quasi-TE^x_{111} modes, respectively; correspondingly, the modes observed at 4.4 GHz and 6.1 GHz are identified as the TE^y_{113} and quasi-TE^x_{113} modes, respectively. The mode frequencies attained by simulation closely corre-

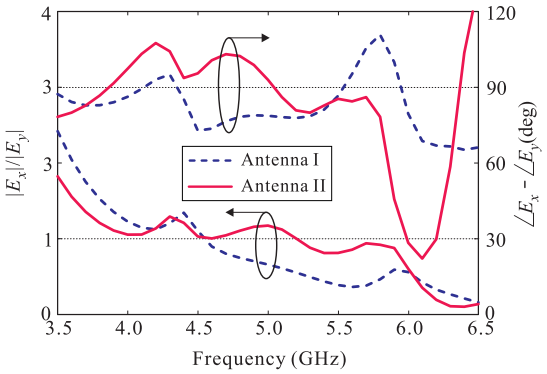

FIGURE 5. Simulated amplitude ratios and phase differences of the radiated electric fields of Antenna I and Antenna II.

spond to those anticipated using the DWM. As observed from Figure 3(b), Antenna I has a minimal AR point at 4.2 GHz, which is almost between the orthogonal degenerate modes TE^{y}_{111} and quasi-TE^{x}_{111}. The 3-dB ARBW of Antenna I is 3.87–4.76 GHz (20.63%). Although the degenerate mode pair of TE^{y}_{113} and quasi-TE^{x}_{113} is excited, these modes do not properly meet the necessary conditions for CP generation, resulting in poor CP radiation with an AR value of ∼6.75 dB at 5.9 GHz.

Antenna II is a modification of Antenna I in which a smaller DR with the optimized dimension of $l1 \times w1 \times h1 = 10.57$ mm $\times$ 4.1 mm $\times$ 11.25 mm is simply added to the sidewall of the main DR. Figure 3 also shows the simulated results of the reflection coefficient and the AR performance of Antenna II. The −10 dB reflection bandwidth of Antenna II is 2.81–5.82 GHz. It was also found that the resonant modes of Antenna II are slightly shifted to a lower frequency range as compared to those of Antenna I due to the presence of the added DR. As observed from Figure 3(b), Antenna II achieves a significantly enhanced 3-dB ARBW of 3.73–5.78 GHz (43.11%), nearly twice that of Antenna I. This is due to the impact of the added DR, which significantly improves the CP radiation of the second orthogonal degenerate mode pair of TE^{y}_{113} and quasi-TE^{x}_{113}, with a subsequent combination with the CP radiation of the first orthogonal degenerate mode pair TE^{y}_{111} and quasi-TE^{x}_{111}, thus achieving broadband CP operation.

In order to generate CP waves, it is necessary to implement two orthogonal electric far-fields with equal amplitude and a 90° phase difference. Figure 5 illustrates the amplitude ratio ($|E_x|/|E_y|$) and the phase difference (PD) ($\angle E_x - \angle E_y$) between the two electric far-fields in the x-axis (E_x) and y-axis (E_y) directions. In Antenna I, the amplitude ratio ($|E_x|/|E_y|$) and PD ($\angle E_x - \angle E_y$) fluctuate between 0.77–1.42 and 73°–95°, respectively, providing a relatively narrow CP bandwidth in the frequency range of 3.87–4.76 GHz. As the frequency increases, the amplitude ratio ($|E_x|/|E_y|$) falls until it is much lower than 1 while the PD fluctuates around 78°. Therefore, poor CP performance is obtained, and the AR value exceeds 3 dB. With the smaller DR added to the main DR, the amplitude ratios ($|E_x|/|E_y|$) of

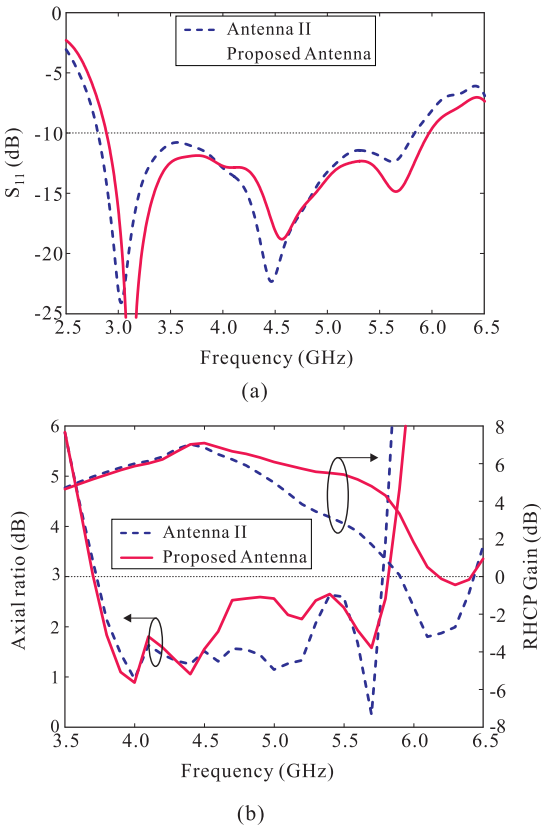

FIGURE 6. Comparison between Antenna II and the proposed antenna in terms of the (a) reflection coefficients and (b) axial ratios and gains.

around 1 are extended to higher frequencies. In the frequency range of 3.73–5.78 GHz, Antenna II has a slowly varying amplitude ratio ($|E_x|/|E_y|$) around 1 (0.82–1.28) and a PD ranging from 80° to 100°, leading to a wider CP bandwidth. These results demonstrate that Antenna II achieves a significantly enhanced 3-dB ARBW as compared to Antenna I.

2) GAIN ENHANCEMENT

Although the 3-dB ARBW Antenna II is significantly enhanced as compared to that of Antenna I, the simulation indicated that the boresight gain of Antenna II at higher frequencies is relative low. Moreover, due to the effect of the added DR, the main beam is tilted away from the $+z$-direction, which also reduces the boresight gain. Therefore, in this subsection, a gain-enhancement technique is applied to Antenna II to realize the proposed wideband CP DRA antenna with high gain performance. It has been experimentally demonstrated [21] that the boresight gain can be improved by increasing the radiation from the sidewalls of a rectangular DRA compared to that from the corresponding top wall. Applying this technique to our design, to increase the radiation intensity from the side walls, a small DR portion with the optimized dimension of $l2 \times w2 \times h2 = 5.5$ mm $\times$ 5.8 mm $\times$ 6.2 mm is removed from a corner of the main rectangular DRA. Figure 6 shows the simulated results of the reflection coefficients, ARs, and

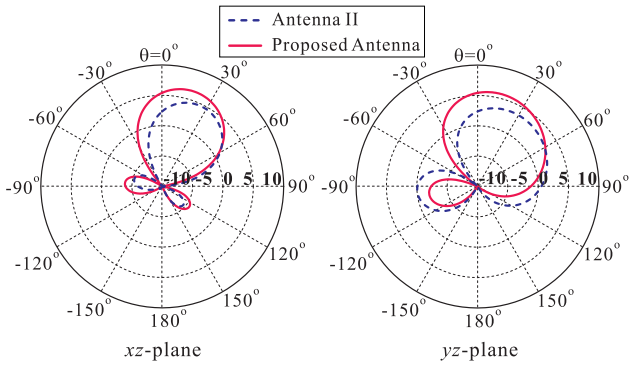

FIGURE 7. Simulated radiation patterns at 5.5 GHz of Antenna II and the proposed antenna on the two cutting planes of *xz*- and *yz*-planes.

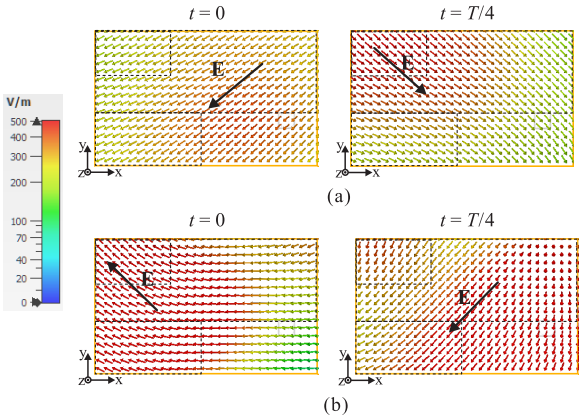

FIGURE 8. Simulated electric field distribution of the proposed antenna observed along the +*z*-direction with time period *T* at (a) 4.0 GHz and (b) 5.7 GHz.

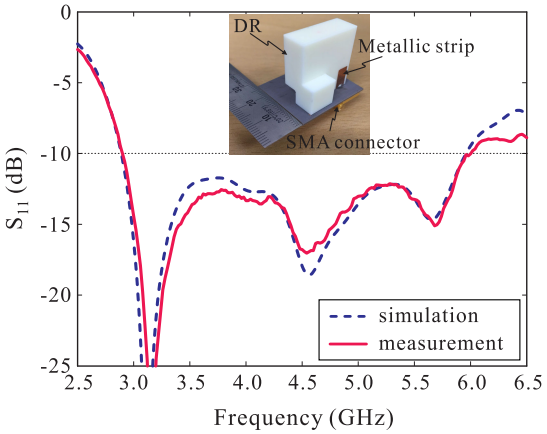

FIGURE 9. Simulated and measured reflection coefficients of the proposed antenna (the fabricated prototype is shown in the inset).

boresight gains of Antenna II and the proposed antenna. It can be seen in Figure 6(a) that the impedance bandwidth is slightly shifted toward a higher frequency after the removal of the small DR portion. The impedance bandwidth for $|S_{11}| \leq -10$ dB for the proposed antenna is 2.89–5.95 GHz (69.23%). As observed in Figure 6(b), the 3-dB ARBWs of the Antenna II and the proposed antenna are similar and are 3.73–5.78 GHz (43.11%) and 3.71–5.82 GHz (44.28%), respectively. These results indicate that the operations of the TE_{111} and TE_{113} modes of the main rectangular DRA are not greatly affected by removing a small DR portion. However, Figure 6(b) clearly shows that the gains in the boresight direction ($\theta = 0°$) of the proposed antenna at higher frequencies are much higher than that of Antenna II. A maximum enhancement of up to 3.0 dBic in boresight gain is attained at 5.5 GHz. Within the 3-dB ARBW, the boresight gains of the proposed antenna range from 4.11 to 7.09 dBic. Figure 7 illustrates the radiation patterns of Antenna II and the proposed antenna at 5.5 GHz on two cutting planes (*xz*- and *yz*-planes). Clearly, when removing the small DR portion, the increased radiation from the side walls not only results in enhanced boresight gain performance but also reduces the beam-tilting effects due to the presence of the added DR.

In order to determine the sense of circular polarization, the electric field distributions with time period T are observed on the top surface of the proposed DRA along the +*z*-direction at 4.0 GHz and 5.7 GHz, as depicted in Figure 8. As shown in Figure 8(a), the electric vector E for $t = 0$ points from the higher right corner to the lower left corner. When t increases from $t = 0$ to $t = T/4$, the electric vector E rotates by 90° in the counterclockwise direction. Similarly, in Figure 8(b), the electric vectors E for $t = 0$ and $t = T/4$ are also orthogonal to each other with a counterclockwise sense of rotation. Therefore, the proposed antenna generates right-handed circular polarization (RHCP) fields in the +*z*-direction throughout the operating bandwidth. It is worth to mention that the sense of CP can be changed from RHCP to LHCP with the proposed antenna by mirroring the antenna structure through the *x*-axis.

IV. EXPERIMENTAL RESULTS AND DISCUSSION

A prototype of the proposed antenna was fabricated for experimental validation. A photograph of the fabricated antenna is shown in the inset of Figure 9. The DR was made of an alumina ceramic material with a dielectric constant of 10 and a loss tangent of 0.0001. The ground plane was mounted onto the bottom surface of a Taconic TLY-5 ($\epsilon_r = 2.2$, $\tan\delta = 0.0009$, and thickness of 0.76 mm) dielectric substrate with a size of 31.5 mm × 27.5 mm. Epoxy adhesive was used to glue the DR to the top surface of the dielectric substrate. The metallic vertical strip was cut from adhesive-backed copper tape to adhere easily onto the DR surface. A SMA connector was soldered onto the metallic strip at the feed point. The S_{11}-parameter was measured using an Agilent 8510C vector network analyzer. The measured and simulated S_{11}-parameters are shown in Figure 9. The measured and simulated impedance bandwidths for $|S_{11}| \leq -10$ dB are 69.66% (2.9–6.0 GHz) and 69.23% (2.89–5.95 GHz), respectively. Good agreement is achieved between the measured and simulated results.

The far-field properties of the proposed antenna, in this case ARs, RHCP gains, and radiation patterns were measured

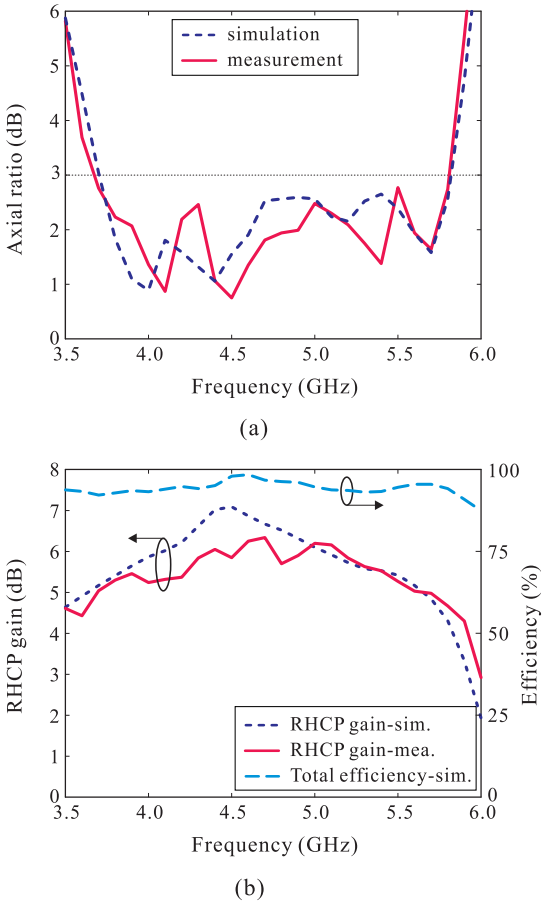

FIGURE 10. Simulated and measured results of the (a) axial ratios and (b) RHCP gains and total efficiency.

in an RF anechoic chamber in which a dual-polarized horn antenna was utilized. The measured and simulated AR in the boresight direction ($\theta = 0°$) provided by the proposed antenna is illustrated in Figure 10(a). As observed, the measured 3-dB ARBW is 3.68–5.80 GHz (44.73%) while the simulated 3-dB ARBW is 3.71–5.82 GHz (44.28%). Note that the measured 3-dB ARBW is entirely covered by the −10 dB impedance bandwidth, resulting in a usable bandwidth of 44.73% (3.68–5.80 GHz) for CP operation. Within the measured 3-dB ARBW, measured RHCP gain ranges from 4.64 to 6.34 dBic, as shown in Figure 10(b). Gain variation of less than 1.7 dBic is obtained in the boresight. Reasonable agreement was noted between the measured and simulated results, with some discrepancies mainly caused by fabrication imperfections and experimental tolerances. Figure 10(b) also shows the simulated total efficiency of the proposed antenna, which remains at more than 88% throughout the passband, with a peak value of 98% at 4.7 GHz. Figure 11 plots the measured and simulated radiation patterns of the proposed antenna on the xz-plane ($\phi = 0°$) and yz-plane ($\phi = 90°$) at the four frequencies of 4.0 GHz, 4.5 GHz, 5.2 GHz, and 5.7 GHz. It is evident that the proposed antenna is an RHCP antenna, and that the radiation patterns are directional toward the boresight direction.

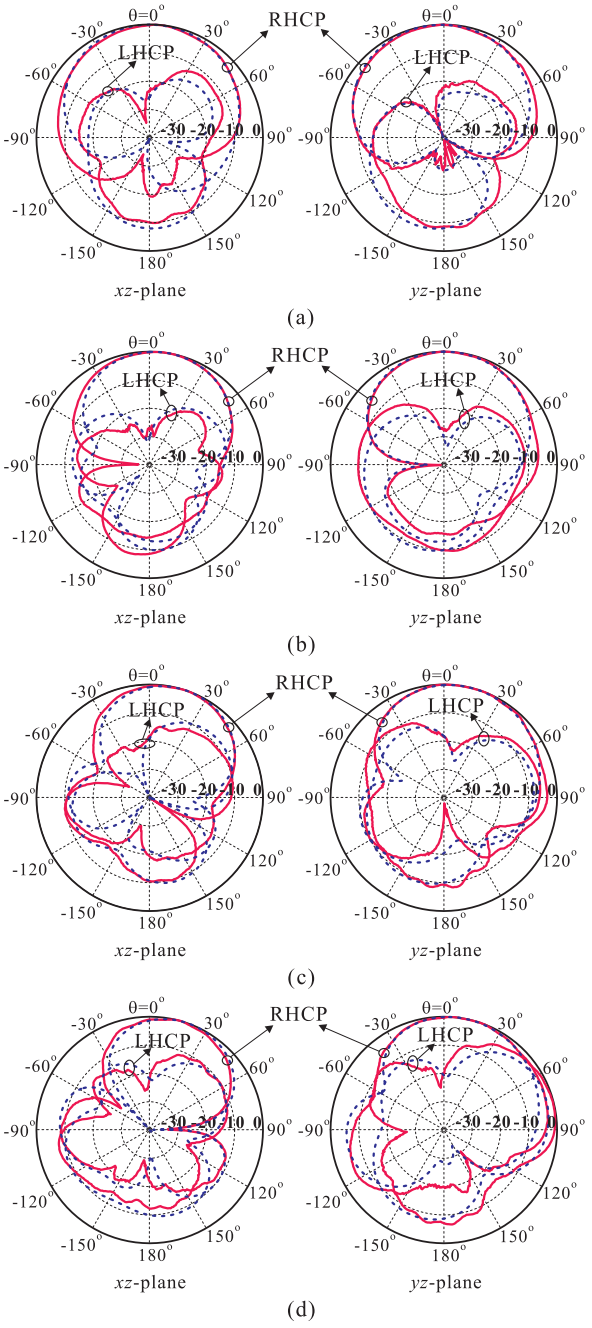

FIGURE 11. Simulated and measured normalized radiation patterns of the proposed antenna at (a) 4.0 GHz, (b) 4.5 GHz, (c) 5.2 GHz, and (d) 5.7 GHz (dotted lines are the simulated results and solid lines are the measured results).

On both planes for these four frequencies, the RHCP gains are approximately 19.5 dB higher than the left-handed circular polarization (LHCP) gains in the boresight direction. In sum, the measured results indicate that the proposed antenna achieves a wide CP bandwidth of 44.73% from 3.68 to 5.80 GHz with a $|S_{11}|$ value of less than −10 dB, an AR level of less than 3 dB, and gain variation less than 1.7 dBic, while the maximum measured RHCP gain is 6.34 dBic at 4.7 GHz. The achieved CP operating frequency band of the proposed antenna covers the operating bandwidths of several

TABLE 1. Comparison between the proposed wideband CP DRA and designs in previous studies.

References	Dimensions $[\lambda_0 \times \lambda_0 \times \lambda_0]$	CP Bandwidth [%]	Peak Gain [dBic]
[14]	1.44×1.44×0.34	14.63	6.13
[15]	1.16×1.16×0.44	21.5	8.39
[16]	0.98×0.98×0.26	22	5.7
[17]	1.48×1.48×0.1	41.01	2
[18]	0.66×0.83×0.39	44.2	5.66
[19]	0.72×0.72×0.18	46.9	4.73
This work	0.50×0.44×0.42	44.73	6.34

λ_0 is the free space wavelength at the center frequency of the passband.

systems, such as WiMAX (3.6–3.8 GHz and 5.25–5.85 GHz) and C-band satellite communications (3.7–4.2 GHz for downlinks). In addition, it is important to note that the proposed antenna can be directly scaled in order to work with any other desired frequency band.

A comprehensive comparison between the proposed wideband CP DRA and designs presented in earlier works [14]–[19] is conducted, as summarized in Table 1. The results of this comparison provide evidence that the proposed antenna has a wider CP bandwidth and a higher gain as compared to the other DRAs [14], [16]–[18]. Although one of these designs [15] has a higher gain, the proposed antenna has a much wider CP bandwidth and a smaller antenna footprint. Compared to one study [19], the proposed antenna provides a slightly narrower CP bandwidth performance but has a much higher gain with a simpler structure.

V. CONCLUSION

A compact single-fed CP DRA with enhanced AR bandwidth and gain characteristics has been designed, fabricated, and measured. The experimental results demonstrate that the proposed CP DRA exhibits a wide 3-dB ARBW of 44.73% (3.68–5.80 GHz), which is entirely covered by a measured −10 dB impedance bandwidth of 69.66% (2.9–6.0 GHz). Within the passband, a measured peak RHCP gain of 6.34 dBic was attained with gain variation of less than 1.7 dBic. The radiation pattern of the proposed CP DRA is directional, and in the broadside direction, the RHCP gain is approximately 19.5 dB more than the LHCP gain. In addition, the proposed antenna has a simple configuration and a straightforward feeding mechanism. Therefore, this antenna can feasibly support various wireless communication systems where a broadband and high-gain CP antenna element is necessary.

REFERENCES

[1] S. Long, M. McAllister, and L. Shen, "The resonant cylindrical dielectric cavity antenna," *IEEE Trans. Antennas Propag.*, vol. AP-31, no. 3, pp. 406–412, May 1983.

[2] K. M. Luk and K. W. Leung, *Dielectric Resonator Antennas*. Baldock, U.K.: Research Studies Press, 2003.

[3] J. Iqbal, U. Illahi, M. I. Sulaiman, M. M. Alam, M. M. Su'ud, M. N. M. Yasin, and M. H. Jamaluddin, "Bandwidth enhancement and generation of CP by using parasitic patch on rectangular DRA for wireless applications," *IEEE Access*, vol. 7, pp. 94365–94372, 2019.

[4] S. Gao, Q. Luo, and F. Zhu, *Circularly Polarized Antennas*. West Sussex, UK.: Wiley, 2014.

[5] X. S. Fang and K. W. Leung, "Linear-/circular-polarization designs of dual-/wide-band cylindrical dielectric resonator antennas," *IEEE Trans. Antennas Propag.*, vol. 60, no. 6, pp. 2662–2671, Jun. 2012.

[6] R.-C. Han, J. Liu, and S.-S. Zhong, "Broadband circularly polarised dielectric resonator antenna fed by wideband switched line coupler," *Electron. Lett.*, vol. 50, no. 10, pp. 725–726, May 2014.

[7] L. C. Y. Chu, D. Guha, and Y. M. M. Antar, "Comb-shaped circularly polarised dielectric resonator antenna," *Electron. Lett.*, vol. 42, no. 14, pp. 785–787, 2006.

[8] J. M. Lee, S.-J. Kim, G. Kwon, C. M. Song, Y. Yang, K.-Y. Lee, and K. C. Hwang, "Circularly polarized semi-eccentric annular dielectric resonator antenna for X-band applications," *IEEE Antennas Wireless Propag. Lett.*, vol. 14, pp. 1810–1813, 2015.

[9] S. Fakhte, H. Oraizi, and R. Karimian, "A novel low-cost circularly polarized rotated stacked dielectric resonator antenna," *IEEE Antennas Wireless Propag. Lett.*, vol. 13, pp. 722–725, 2014.

[10] M. I. Sulaiman and S. K. Khamas, "A singly fed wideband circularly polarized dielectric resonator antenna using concentric open half-loops," *IEEE Antennas Wireless Propag. Lett.*, vol. 10, pp. 1305–1308, 2011.

[11] J. M. Lee, G. Kwon, C. M. Song, K.-Y. Lee, Y. Yang, and K. C. Hwang, "Wideband circularly polarized spidron fractal slot antenna with a grooved dielectric resonator," *J. Electromagn. Waves Appl.*, vol. 29, no. 14, pp. 1942–1951, Aug. 2015.

[12] M. Zou and J. Pan, "Wideband hybrid circularly polarised rectangular dielectric resonator antenna excited by modified cross-slot," *Electron. Lett.*, vol. 50, no. 16, pp. 1123–1125, Jul. 2014.

[13] R. Chowdhury, N. Mishra, M. M. Sani, and R. K. Chaudhary, "Analysis of a wideband circularly polarized cylindrical dielectric resonator antenna with broadside radiation coupled with simple microstrip feeding," *IEEE Access*, vol. 5, pp. 19478–19485, 2017.

[14] S. Trinh-Van, Y. Yang, K.-Y. Lee, and K. Hwang, "A wideband circularly polarized pixelated dielectric resonator antenna," *Sensors*, vol. 16, no. 9, pp. 1349–1355, Aug. 2016.

[15] Y. Pan and K. W. Leung, "Wideband circularly polarized trapezoidal dielectric resonator antenna," *IEEE Antennas Wireless Propag. Lett.*, vol. 9, pp. 588–591, 2010.

[16] S. Fakhte, H. Oraizi, R. Karimian, and R. Fakhte, "A new wideband circularly polarized stair-shaped dielectric resonator antenna," *IEEE Trans. Antennas Propag.*, vol. 63, no. 4, pp. 1828–1832, Apr. 2015.

[17] G. Varshney, V. S. Pamdey, R. S. Yaduvanshi, and L. Kumar, "Wideband circularly polarized dielectric resonator antenna with stair-shaped slot excitation," *IEEE Trans. Antennas Propag.*, vol. 65, no. 3, pp. 1380–1383, Mar. 2017.

[18] A. Altaf, J.-W. Jung, Y. Yang, K.-Y. Lee, and K. Hwang, "Vertical-strip-fed broadband circularly polarized dielectric resonator antenna," *Sensors*, vol. 17, no. 8, pp. 1911–1919, Aug. 2017.

[19] M. Yang, Y. Pan, and W. Yang, "A singly fed wideband circularly polarized dielectric resonator antenna," *IEEE Antennas Wireless Propag. Lett.*, vol. 17, no. 8, pp. 1515–1518, Aug. 2018.

[20] R. Kumar Mongia and A. Ittipiboon, "Theoretical and experimental investigations on rectangular dielectric resonator antennas," *IEEE Trans. Antennas Propag.*, vol. 45, no. 9, pp. 1348–1356, Sep. 1997.

[21] S. Fakhte, H. Oraizi, and L. Matekovits, "Gain improvement of rectangular dielectric resonator antenna by engraving grooves on its side walls," *IEEE Antennas Wireless Propag. Lett.*, vol. 16, pp. 2167–2170, 2017.

SON TRINH-VAN was born in Hanoi, Vietnam, in 1986. He received the B.Sc. (Eng.) degree in electronics and telecommunications from the Hanoi University of Science and Technology, Hanoi, in 2010, and the Ph.D. degree from the Division of Electronics and Electrical Engineering, Dongguk University, Seoul, South Korea, in 2015. He is currently a Postdoctoral Researcher with the Department of Electrical and Computer Engineering, Sungkyunkwan University, Suwon, South Korea. His research interest includes design of circularly polarized antennas and millimeter-wave antennas and arrays.

YOUNGOO YANG (Member, IEEE) was born in Hamyang, South Korea, in 1969. He received the Ph.D. degree in electrical and electronic engineering from the Pohang University of Science and Technology (POSTECH), Pohang, South Korea, in 2002. From 2002 to 2005, he was with Skyworks Solutions Inc., Newbury Park, CA, USA, where he designed power amplifiers for various cellular handsets. Since March 2005, he has been with the School of Information and Communication Engineering, Sungkyunkwan University, Suwon, South Korea, where he is currently a Professor. His research interests include RF/mm-wave power amplifiers, RF transmitters, and dc–dc converters.

KANG-YOON LEE received the B.S., M.S., and Ph.D. degrees from the School of Electrical Engineering, Seoul National University, Seoul, South Korea, in 1996, 1998, and 2003, respectively. From 2003 to 2005, he was with GCT Semiconductor Inc., San Jose, CA, USA, where he was a Manager of the Analog Division and worked on the design of CMOS frequency synthesizer for CDMA/PCS/PDC and single-chip CMOS RF chip sets for W-CDMA, WLAN, and PHS. From 2005 to 2011, he was an Associate Professor with the Department of Electronics Engineering, Konkuk University. Since 2012, he has been with the School of Information and Communication Engineering, Sungkyunkwan University, where he is currently an Associate Professor. His research interests include implementation of power integrated circuits, CMOS RF transceiver, analog integrated circuits, and analog/digital mixed-mode VLSI system design.

KEUM CHEOL HWANG (Senior Member, IEEE) received the B.S. degree in electronics engineering from Pusan National University, Busan, South Korea, in 2001, and the M.S. and Ph.D. degrees in electrical and electronic engineering from the Korea Advanced Institute of Science and Technology (KAIST), Daejeon, South Korea, in 2003 and 2006, respectively.

From 2006 to 2008, he was with Samsung Thales, Yongin, South Korea, where he was involved with the development of various antennas for wireless communications and radar systems. From 2008 to 2014, he was an Associate Professor with the Division of Electronics and Electrical Engineering, Dongguk University, Seoul, South Korea. In 2015, he joined the Department of Electrical and Computer Engineering, Sungkyunkwan University, Suwon, South Korea, where he is currently a Professor. His research interests include advanced electromagnetic scattering and radiation theory and applications, design of multiband/broadband array antennas, and optimization algorithms for electromagnetic applications.

Dr. Hwang is a member of IEICE and a Life Member of KIEES.